Journal of Hepatocellular Carcinoma

Dovepress
Taylor & Francis Group

Open Access Full Text Article

ORIGINAL RESEARCH

MRI Radiomics-Based Evaluation of Vessels Encapsulating Tumor Clusters and Microvascular Invasion in Hepatocellular Carcinoma

Yanyi Liu[1], Yanyan Zhang[1], Xinxin Wang[2], Hanyu Jiang[3], Wei Wang[1], Hongjun Li[1,4]

[1]Department of Radiology, Beijing Youan Hospital, Capital Medical University, Beijing, People's Republic of China; [2]Department of Pathology, Beijing Youan Hospital, Capital Medical University, Beijing, People's Republic of China; [3]Department of Radiology, West China Hospital of Sichuan University, Chengdu, People's Republic of China; [4]Joint Laboratory for Basic and Clinical Research on Virus-Associated Liver Diseases, Capital Medical University, Beijing, People's Republic of China

Correspondence: Hongjun Li, Department of Radiology, Beijing Youan Hospital, Capital Medical University, No. 8 Xi Tou Tiao, Youanmen Wai, Fengtai District, Beijing, 100069, People's Republic of China, Email lihongjun00113@ccmu.edu.cn

Purpose: This study aimed to develop a radiomics model based on dynamic contrast-enhanced magnetic resonance imaging (DCE-MRI) for the preoperative prediction of two distinct histopathological vascular patterns in hepatocellular carcinoma (HCC): vessels encapsulating tumor clusters (VETC) and microvascular invasion (MVI). In addition, the study evaluated the prognostic significance of these vascular patterns in predicting postoperative outcomes in patients with HCC.

Patients and Methods: A total of 306 patients with HCC who underwent radical resection at two medical centers were retrospectively included. Patients from Center 1 were randomly assigned to a training cohort and an internal validation cohort at a ratio of 7:3, while patients from Center 2 comprised the external validation cohort. Radiomics features were extracted from the arterial phase (AP), portal venous phase (PP), and delayed phase (DP) DCE-MRI images, including intratumoral, peritumoral, and fused intra-peritumoral regions. Radiomics models were constructed based on these features, and the optimal model was subsequently integrated with clinical variables to establish a combined clinical–radiomics model.

Results: For predicting VETC and/or MVI (defined as VM patterns), the combined model achieved area under the curve (AUC) values of 0.857 in the training cohort, 0.761 in the internal validation cohort, and 0.723 in the external validation cohort. Calibration and decision curve analysis (DCA) indicated acceptable calibration performance and potential clinical utility of the combined model. Both pathological VM positivity and model-predicted VM positivity were significantly associated with early recurrence (ER) and shorter disease-free survival (DFS).

Conclusion: The clinical–radiomics combined model based on DCE-MRI holds potential value as a noninvasive preoperative approach for evaluating VM patterns and postoperative prognosis in patients with HCC.

Keywords: hepatocellular carcinoma, radiomics, VETC, MVI, DCE-MRI, prognosis

Introduction

Primary liver cancer ranks as the sixth most common malignancy and the third leading cause of cancer-related mortality worldwide. Among primary liver cancers, HCC accounts for the vast majority.[1] For patients with preserved liver function, curative hepatectomy remains the standard first-line treatment.[2] However, despite surgical intervention, the five-year overall survival rate is approximately 70%, with recurrence rates exceeding 80%.[3] Identifying reliable predictors of postoperative recurrence therefore represents a critical unmet clinical need.

Tumor vascular architecture plays a pivotal role in HCC progression and dissemination.[4] Previous studies have described two distinct vascular patterns associated with poor prognosis in HCC, namely MVI and VETC.[5,6] The development of MVI depends on epithelial-mesenchymal transition (EMT) and reflects tumor cell invasion into microvessels. MVI has been widely recognized as an important predictor of early recurrence and metastasis.[7]

https://doi.org/10.2147/JHC.S578689
Received: 8 November 2025
Accepted: 13 March 2026
Published: 27 March 2026

However, in clinical practice, a substantial proportion of patients still experience recurrence and metastasis after radical resection even without such key invasive feature. Studies have found that VETC is a novel metastatic mechanism distinct from EMT, emphasizing the specific encapsulation of tumor cell clusters by blood vessels.[8] On the morphological level of pathology, VETC is characterized by tumor clusters surrounded by CD34-positive vascular endothelial cells, and these tumor clusters can directly enter the circulation through anastomoses with surrounding blood vessels, thereby facilitating metastasis.[9,10] By contrast, MVI refers to the presence of tumor emboli in small vascular lumens lined by endothelial cells.[11,12] VETC provides an important supplement to MVI in describing the heterogeneity of HCC recurrence.[5] Accordingly, combined evaluation of MVI and VETC may more comprehensively reflect tumor biology and improve preoperative risk assessment.

However, preoperative prediction of VETC and MVI remains challenging, as these pathological features can only be confirmed through histopathological examination of resected specimens. Imaging plays a pivotal role in the routine diagnosis and evaluation of HCC, with MRI offering superior soft-tissue contrast and functional imaging capability that enables comprehensive assessment of tumor characteristics.[13] Recent advances in medical image analysis have enabled the extraction of high-throughput quantitative features from imaging data. Radiomics, as an emerging technique, provides a non-invasive approach to characterize the underlying pathophysiological features of tumors.[14,15] Several MRI-based radiomics studies have reported promising performance in predicting either MVI or VETC individually.[16,17]

Despite the progress made in existing studies, no standardized preoperative MRI-based diagnostic model for predicting HCC-VM patterns has been established to date. Based on this, relying on a two-center retrospective cohort, this study focused on the radiomics features of intratumoral and peritumoral regions in the arterial phase of MRI as well as key clinical features, ultimately constructing a prediction model for VM patterns, and improving the stability and clinical applicability of the model through strict external validation.

Materials and Methods

Patients

In Center 1, consecutive patients with HCC who underwent curative liver resection between September 2013 and April 2024 were retrospectively enrolled. The inclusion criteria were as follows: (1) histopathological confirmation of HCC; (2) DCE-MRI performed within two months before surgery; (3) availability of surgical pathology specimens; and (4) availability of complete clinical and laboratory data. The exclusion criteria were: (1) previous treatment for HCC, including chemotherapy, radiotherapy, transarterial chemoembolization (TACE), radiofrequency ablation, or liver transplantation; (2) presence of distant metastasis, major vascular invasion, tumor thrombosis, or other concomitant malignancies; (3) poor image quality on MRI or inadequate quality of pathology slides; and (4) tumors with a maximum diameter <10 mm. The final cohort from Center 1 was randomly divided into an internal training cohort and an internal validation cohort in a 7:3 ratio. Patients from Center 2 who underwent liver resection between August 2012 and December 2020 were enrolled as an external validation cohort using the same inclusion and exclusion criteria. In patients with multiple lesions, the largest tumor was selected as the primary lesion for analysis. Tumors smaller than 10 mm were excluded to ensure segmentation accuracy and feature stability, but it may limit the applicability of the model to subcentimeter HCCs. Patients were classified according to their VETC and MVI status into VM-positive HCC (VM-HCC+) and VM-negative HCC (VM-HCC-) groups. VM-HCC+ included tumors with any of the following combinations: VETC+/MVI+, VETC+/MVI-, and VETC-/MVI+, whereas VM-HCC^{-} referred to tumors negative for both VETC and MVI (VETC-/MVI-)(Figure 1).

Baseline clinical characteristics, including age, sex, tumor number and size, cirrhosis status, etiology of liver disease, Barcelona Clinic Liver Cancer (BCLC) stage, and Child–Pugh score, were recorded. Laboratory data, including alanine aminotransferase (ALT), aspartate aminotransferase (AST), γ-glutamyl transferase (GGT), serum albumin (ALB), total bilirubin (TBil), prothrombin time (PT), platelet count (PLT), and serum alpha-fetoprotein (AFP), were collected from electronic medical records.

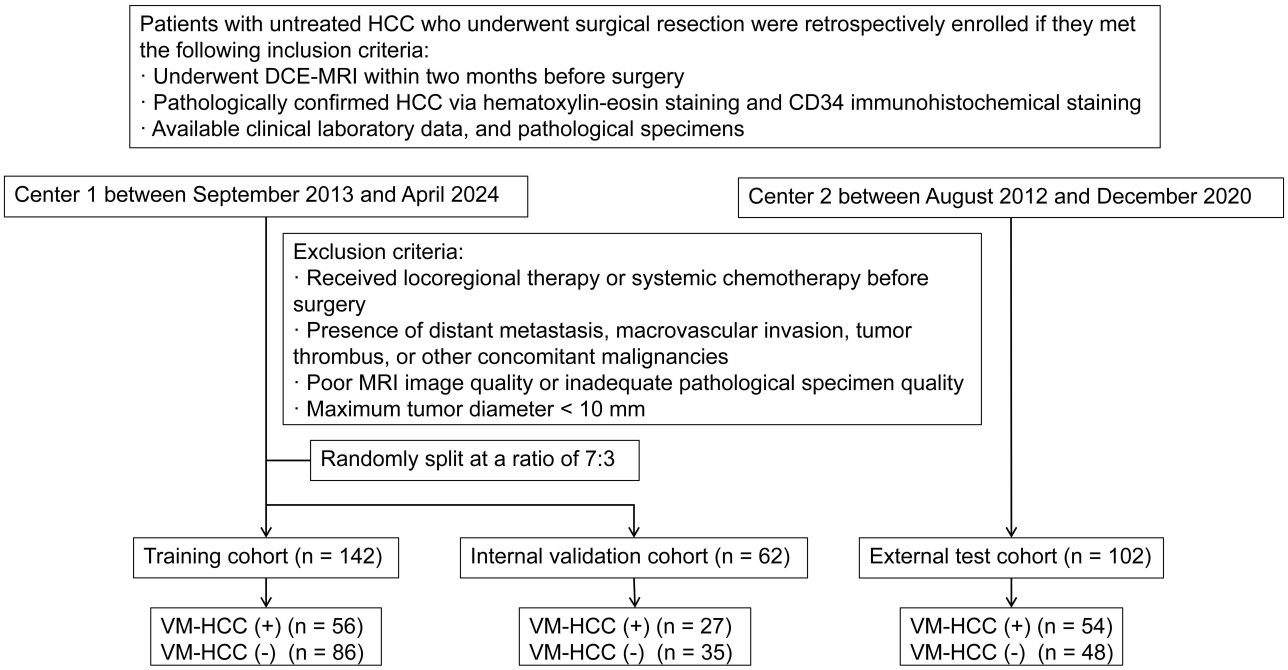

Figure 1 Flowchart demonstrating recruitment pathway for the population.
Abbreviations: HCC, hepatocellular carcinoma; VETC, vessels encapsulating tumor clusters; MVI, microvascular invasion; VM, VETC-MVI; VM-HCC+ (VETC+/MVI+, VETC-/MVI+, VETC+/MVI-) and VM-HCC- (VETC-/MVI-).

Histopathology and Immunohistochemistry

The reference standards for MVI and VETC were established based on pathological assessment of resected specimens (Figure 2). All slides were independently reviewed by two experienced hepatopathologists who were blinded to the clinical and imaging data. In cases of disagreement, a final diagnosis was established by consensus after joint review and discussion.

MVI was evaluated using hematoxylin and eosin (H&E)–stained sections, whereas VETC was determined by CD34 immunohistochemical staining. The diagnostic criteria for VETC were defined as tumor cell clusters completely encapsulated by a network of CD34-positive sinusoidal endothelial cells. The extent of VETC was assessed in 5%

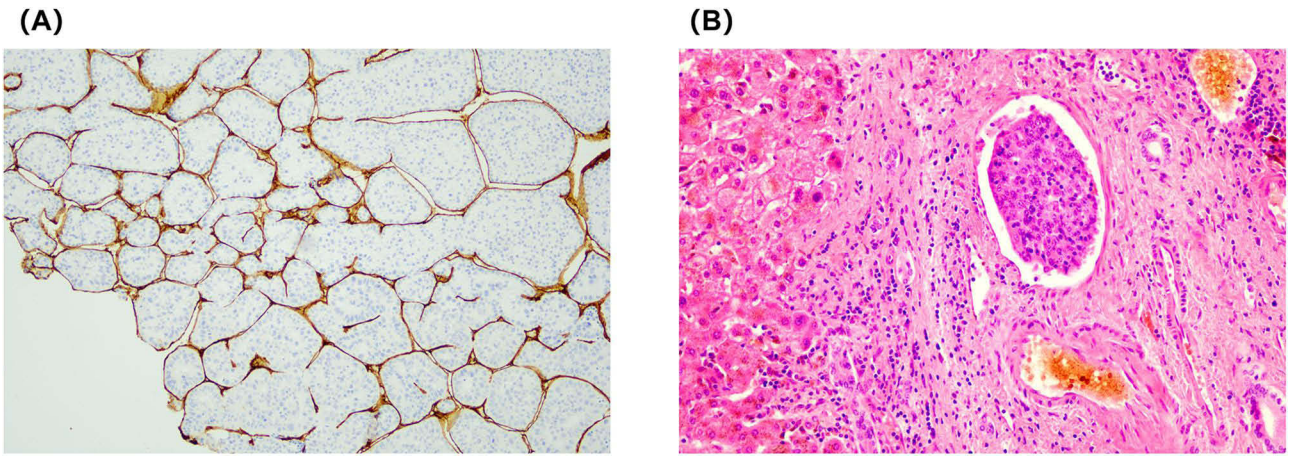

Figure 2 Pathological criteria for VETC and MVI positivity.
Notes: (**A**) VETC positivity was defined as the presence of tumour cell clusters completely encircled by sinusoid-like, endothelial-lined vascular channels forming a continuous cobweb-like network. Original magnification ×100. (**B**) MVI positivity was defined as microscopic evidence, on H&E stained sections, of tumour cell nests located within an endothelial-lined vascular lumen in the peritumoral or capsular microvasculature. Original magnification ×200.
Abbreviations: HCC, hepatocellular carcinoma; VETC, vessels encapsulating tumor clusters; MVI, microvascular invasion.

https://doi.org/10.2147/JHC.S578689

increments per field. According to a previous multicenter study,[9] VETC positivity was defined as ≥55% of the tumor surface area being covered by VETC structures (range, 0–100%). MVI was defined as the presence of tumor cell clusters within vascular lumens lined by endothelial cells under light microscopy.[18]

Follow-Up

All patients were followed up every 3 to 6 months after surgery using serum AFP testing and contrast-enhanced computed tomography (CT) or MRI to monitor for recurrence, metastasis, and disease progression. Follow-up ended in November 2024 or at the time of disease progression. For patients lost to follow-up, survival time was calculated from the date of surgery to the last available follow-up visit. ER was defined as the appearance of new lesions with imaging features consistent with HCC within two years after curative resection. DFS was defined as the time interval between curative resection and disease progression.

MRI Protocol

DCE-MRI was performed using a 3.0-T scanner equipped with either an 8-channel body coil (TIM TRIO, Siemens, Erlangen, Germany) or an 18-channel phased-array body coil and a spine coil (Magnetom Skyra, Siemens Healthineers, Erlangen, Germany). Prior to scanning, patients fasted for 4–6 hours and subsequently received an intravenous bolus injection of gadobenate dimeglumine (Gd-BOPTA) at a dose of 0.1 mmol/kg, administered at a rate of 2.5 mL/s. T1-weighted (T1WI), T2-weighted (T2WI), and diffusion-weighted (DWI) images were acquired. Arterial phase (AP), portal venous phase (PVP), and delayed phase (DP) images were obtained at approximately 20–30 s, 50–60 s, and 90–120 s after contrast injection, respectively. MRI scanning protocols followed the recommendations of the 2018 American Association for the Study of Liver Diseases (AASLD) guidelines. Detailed MRI acquisition parameters are summarized in Supplemental Table 1.

Radiomics Feature Extraction and Selection

The workflow for radiomics feature extraction is illustrated in Figure 3. Before segmentation, all images underwent N4 bias field correction. Two radiologists from different medical institutions, each with 5 years of experience in abdominal imaging, independently delineated the region of interest (ROI) on the arterial phase, portal venous phase, and delayed phase DCE-MRI images using ITK-SNAP software (version 4.2.0; www.itksnap.org). A senior radiologist with 10 years of experience reviewed all segmentations to ensure accuracy and consistency. The intratumoral region was defined as the area within the tumor boundary, and a 5-mm margin was expanded outward from the tumor to define the peritumoral region, excluding areas outside the liver parenchyma. In addition, another radiologist with 3 years of experience randomly selected 50 cases for independent segmentation to assess interobserver reproducibility. Radiomics features from both intratumoral and peritumoral regions were extracted using the open-source PyRadiomics Python package (https://pyradiomics.readthedocs.io). Feature extraction was performed on resampled isotropic voxels ($1\times1\times1$ mm^3) with an intensity bin width of 5. Wavelet and Laplacian of Gaussian (LoG) filters with $\sigma = 3.0$ and 5.0 were applied to both the original and preprocessed images. Extracted features included shape, first-order statistics, and texture features derived from gray-level co-occurrence matrix (GLCM), gray-level run-length matrix (GLRLM), gray-level size-zone matrix (GLSZM), gray-level dependence matrix (GLDM), and neighborhood gray-tone difference matrix (NGTDM). All feature definitions complied with the Image Biomarker Standardization Initiative (IBSI) guidelines.[19]

After feature extraction, radiomics features were harmonized using the ComBat method with center as the batch variable. Subsequently, feature selection was conducted in four steps: (1) Features with an intraclass correlation coefficient (ICC) < 0.8 were excluded to ensure reproducibility. (2) Z-score normalization was applied, and features with significant differences between groups ($P < 0.05$) identified by the Mann–Whitney *U*-test or Student's *t* test were retained. (3) To minimize multicollinearity, the Pearson correlation matrix of the remaining features was calculated, and among highly correlated pairs ($|r| > 0.9$), the feature most strongly correlated with the target variable or with greater clinical relevance was preserved. (4) Finally, the least absolute shrinkage and selection operator (LASSO) regression was applied for dimensionality reduction to identify the most informative features. The penalty parameter (λ) was optimized using 10-fold cross-validation. The radiomics score (RAD-score) for each patient was calculated as a linear combination of the selected features weighted by their respective LASSO coefficients.

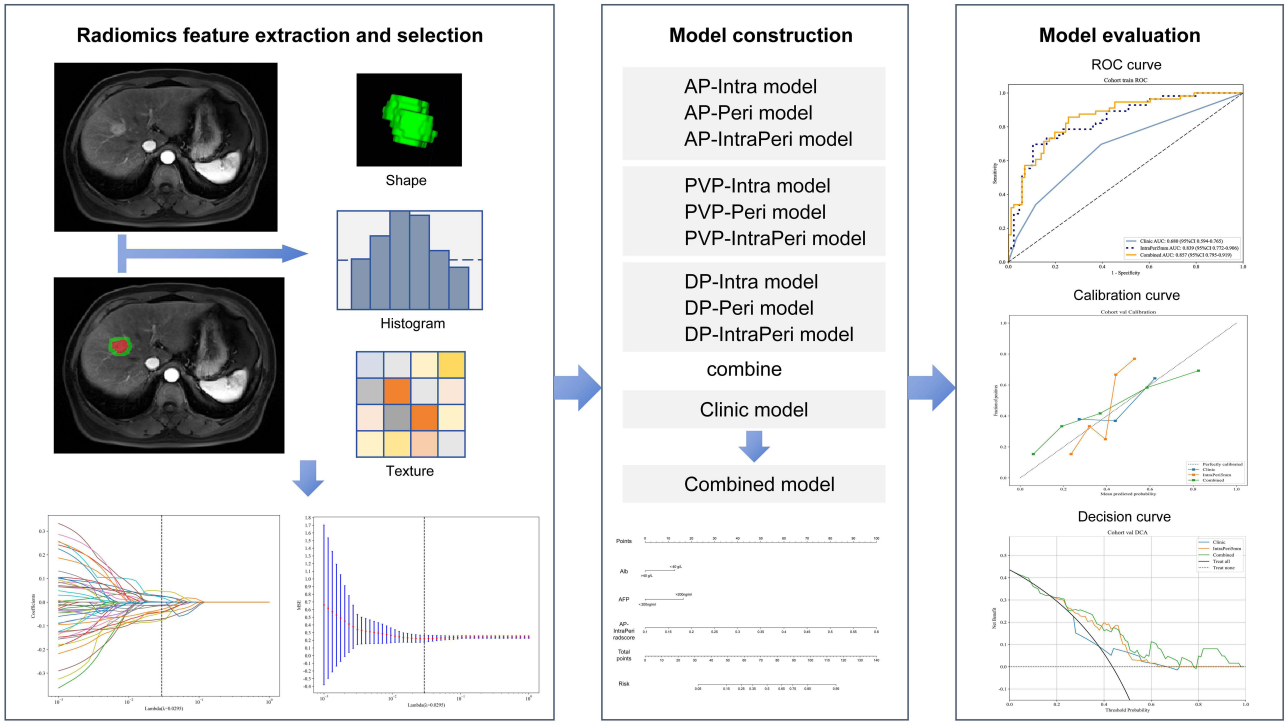

Figure 3 Workflow for radiomics feature extraction, model construction, and model evaluation.
Notes: The blue arrows indicate the workflow and direction of data flow throughout the analysis. The horizontal arrows connect the three main stages from radiomics feature extraction and selection to model construction and subsequent model evaluation, while the vertical arrows denote the next sub-step within a stage (e.g., feature selection after ROI delineation and generation of the combined model after integrating radiomics and clinical variables). Intra model, a model that combines features from single-sequence images within the tumor. Peri model, a model that combines features from single-sequence images surrounding the tumor. IntraPeri model, a model that integrates features from both the tumor and its surrounding microenvironment, incorporating characteristics from intra-tumoral and peri-tumoral single-sequence images.
Abbreviations: HCC, hepatocellular carcinoma; VETC, vessels encapsulating tumor clusters; MVI, microvascular invasion; VM, VETC-MVI; VM-HCC+ (VETC+/MVI+, VETC-/MVI+, VETC+/MVI-) and VM-HCC- (VETC-/MVI-). AP, arterial phase; PP, portal venous phase; DP delayed phase. ROI, region of interest.

Model Construction

Patients from Center 1 were randomly divided into a training cohort and an internal validation cohort in a 7:3 ratio, while patients from Center 2 were used as an external independent validation cohort. Univariate and multivariate logistic regression analyses were performed to identify variables associated with VM-HCC. Multicollinearity among variables was assessed using the variance inflation factor (VIF), and variables with VIF ≤ 5 and $p < 0.05$ were included in the construction of the clinical model.

Based on these groupings, nine radiomics models were built to predict VM-HCC status, including models derived from intratumoral and peritumoral regions in the AP, portal PVP, and DP of DCE-MRI, as well as three pre-fusion models integrating tumor and peritumoral features. A separate clinical model was developed from significant clinical predictors. The predictive performance of all radiomics models was compared, and the model with the highest AUC was combined with the clinical model to create an integrated clinical–radiomics model. The entire feature-selection and model-building pipeline was performed exclusively in the training cohort, and the frozen model was subsequently applied to the internal and external validation cohorts. The optimal cut-off value of the combined model was determined by Youden's index in the training cohort, and fixed for all validation analyses without re-optimization.

The independent clinical predictors were determined by multivariate logistic regression analysis. A nomogram based on the optimal predictive model was constructed to visualize the probability of VM-HCC. All codes used for model construction are publicly available on GitHub (https://github.com/OnekeyAI-Platform/robstene).

https://doi.org/10.2147/JHC.S578689

Statistical Analysis

Continuous variables were compared using the Mann–Whitney *U*-test, while categorical variables were compared using the χ^2-test or Fisher's exact test, as appropriate. Univariate logistic regression was used to identify potential predictors, and multivariate logistic regression was applied to determine independent predictors, with odds ratio (OR) and 95% confidence interval (CI) calculated. The discriminative ability of each model was evaluated by the AUC, and differences between AUCs were assessed using DeLong's test. Calibration performance was evaluated using calibration curves, and DCA was conducted to assess the net clinical benefit across a range of threshold probabilities. Survival outcomes were analyzed using the Kaplan–Meier method, and differences between survival curves were compared using the Log rank test. All univariate and multivariate analyses, as well as survival analyses, were performed using R software (version 4.5.1; www.R-project.org). Model construction and performance evaluation were carried out using Python (version 3.11; www.python.org). All statistical tests were two-sided, and $p < 0.05$ was considered statistically significant.

Results

Patient Characteristics and Clinical Factors

The baseline demographic and clinical characteristics of all patients are summarized in Table 1. A total of 306 patients were included in this study (mean age, 54.9 ± 10.2 years; 254 men and 52 women). Most patients (262 of 306, 85%) were infected with hepatitis B virus (HBV), and 175 (57%) had underlying liver cirrhosis. Histopathological assessment showed that the distribution of VM status was balanced among the training, internal validation, and external validation cohorts (P = 0.37). In the training cohort, patients with VM-HCC+ were more likely to have an elevated AFP level > 200 ng/mL than those with VM-HCC-(19 of 56 [34%] vs. 10 of 86 [12%]; P = 0.001), and they exhibited a lower serum ALB

Table 1 Baseline Characteristics of the Study Population

Characteristics	Training Cohort (n=142)			Internal Validation Cohort (n = 62)			External Test Cohort (n = 102)		
	VM-HCC (+) (n = 56)	VM-HCC (-) (n = 86)	P Value	VM-HCC (+) (n = 27)	VM-HCC (-) (n = 35)	P Value	VM-HCC (+) (n = 54)	VM-HCC (-) (n = 48)	P Value
Age	54.77±9.16	53.44±10.26	0.464	56.63±8.81	58.34±10.49	0.497	53.33±10.32	55.79±11.01	0.308
Male sex (%)	46(82.14)	70(81.40)	1	22(81.48)	28(80.00)	1	46(85.19)	42(87.50)	0.959
Aetiology (%)			1			1			0.420
HBV	46(82.14)	71(82.56)		25(92.59)	33(94.29)		48(88.89)	39(81.25)	
Other	10(17.86)	15(17.44)		2(7.41)	2(5.71)		6(11.11)	9(18.75)	
Cirrhosis (%)	31(55.36)	41(47.67)	0.470	18(66.67)	23(65.71)	1	36(66.67)	26(54.17)	0.277
Child-Pugh (%)			0.415			1			1
A	56(100.00)	83(96.51)		26(96.30)	33(94.29)		54(100.00)	48(100.00)	
B or C	Null	3(3.49)		1(3.70)	2(5.71)		null	null	
BCLC stage (%)			0.709			0.362			1
0 or A	51(91.07)	81(94.19)		25(92.59)	35(100.00)		54(100.00)	48(100.00)	
B or C	5(8.93)	5(5.81)		2(7.41)	Null		Null	Null	
ALT >50 U/L (%)	9(16.07)	8(9.30)	0.342	4(14.81)	3(8.57)	0.715	11 (20.37)	11(22.92)	0.943
AST >40 U/L (%)	8(14.29)	15(17.44)	0.790	6(22.22)	4(11.43)	0.425	20(37.04)	11(22.92)	0.183
GGT >45 U/L (%)	18(32.14)	28(32.56)	1	12(44.44)	11(31.43)	0.431	30(55.56)	17(35.42)	0.066
ALB >40 g/L (%)	28(50.00)	59(68.60)	0.041	16(59.26)	21(60.00)	1	42(77.78)	42(87.50)	0.305
PT >13s	4(7.14)	8(9.30)	0.886	3(11.11)	6(17.14)	0.760	8(14.81)	5(10.42)	0.713
PLT (>100) (%)	46(82.14)	68(79.07)	0.815	20(74.07)	22(62.86)	0.507	35(64.81)	32(66.67)	1
AFP >200ng/mL (%)	19(33.93)	10(11.63)	0.003	9(33.33)	5(14.29)	0.141	21(38.89)	11(22.92)	0.128
Tbil>20μmol/L (%)	15(26.79)	19(22.09)	0.661	8(29.63)	10(28.57)	1	10(18.52)	7(14.58)	0.790
Tumor number			0.470			0.362			0.158
1	47(83.93)	77(89.53)		25(92.59)	35(100.00)		53(98.15)	43(89.58)	
> =2	9(16.07)	9(10.47)		2(7.41)	Null		1(1.85)	5(10.42)	
Main tumor size (mean [SD]) (cm)	3.05±1.81	2.60±1.44	0.071	3.88±2.16	2.54±1.32	0.004	5.03±2.07	3.27±1.37	<0.001

Abbreviations: HCC, hepatocellular carcinoma; VETC, vessels encapsulating tumor clusters; MVI, microvascular invasion; VM, VETC-MVI; VM-HCC+ (VETC+/MVI+, VETC-/MVI+, VETC+/MVI-); VM-HCC- (VETC-/MVI-); HBV, hepatitis B virus; BCLC, Barcelona Clinic Liver Cancer; ALT, alanine aminotransferase; AST, aspartate aminotransferase; GGT, gamma-glutamyl transferase; ALB, albumin; PT, prothrombin time; PLT, platelet; AFP, alpha-fetoprotein; Tbil, total bilirubin; SD, standard deviation.

level (28 of 56 [50%] vs. 59 of 86 [68.6%]; P = 0.026). No significant differences were found between the two groups in other clinical or laboratory parameters (P = 0.230–0.959). In both the internal and external validation cohorts, the maximum tumor diameter differed significantly between the VM-HCC+ and VM-HCC- groups (P = 0.003 and P < 0.001, respectively). However, AFP and ALB levels did not differ significantly between the groups in these two cohorts. Multivariate logistic regression analysis identified AFP and ALB as independent predictors of VM-HCC (Table 2).

Radiomics Feature Extraction and Selection

A total of 2031 radiomics features were extracted from each DCE-MRI phase (arterial, portal venous, and delayed). To mitigate inter-center batch effects, ComBat harmonization was performed using study center as the batch variable. Principal component analysis (PCA) demonstrated no obvious center-driven clustering after harmonization (Supplemental Figure 1). The harmonized features were then Z-score standardized and subjected to an initial univariate screening using either the Mann–Whitney *U*-test or Student's *t* test, as appropriate based on data distribution.

To further reduce redundancy and multicollinearity, features with a Pearson correlation coefficient $|r|>0.9$ were removed, resulting in 54 nonredundant features. Subsequently, least absolute shrinkage and selection operator (LASSO) regression was applied for dimensionality reduction, yielding 14 optimal features. These features were used to construct the radiomics model and calculate the Rad-score (Supplemental Figure 2A and 2B). The relative contribution of each

Table 2 Univariate and Multivariate Analysis for VM-HCC in the Training Cohort

Characteristics	Univariate Analysis		Multivariate Analysis	
	OR (95% CI)	P Value	OR (95% CI)	P Value
Age> 55 years	1.048(0.534–2.058)	0.892		
Sex	1.051(0.444–2.588)	0.910		
Aetiology	0.972(0.406–2.409)	0.949		
Cirrhosis	1.361(0.694–2.690)	0.370		
AFP>200ng/mL	3.903(1.682–9.543)	0.001	4.170 (1.762–10.447)	0.001
ALT >50 U/L	1.867(0.670–5.295)	0.230		
AST>40 U/L	0.789(0.297–1.965)	0.616		
GGT >45 U/L	0.981(0.473–2.007)	0.959		
ALB>40 g/L	0.458(0.227–0.913)	0.026	0.424 (0.203–0.872)	0.020
PT>13s	0.750(0.192–2.511)	0.648		
PLT>10^9/L	1.218(0.524–2.963)	0.651		
Tbil>20μmol/L	1.290(0.585–2.814)	0.524		
Tumor number	1.638(0.599–4.484)	0.331		
Main tumor size	1.189(0.964–1.482)	0.106		
Child-Pugh	NA	NA		
BCLC stage	1.588(0.423–5.973)	0.483		

Notes: Data in parentheses are 95% confidence intervals (CIs).
Abbreviations: HCC, hepatocellular carcinoma; VETC, vessels encapsulating tumor clusters; MVI, microvascular invasion; VM, VETC-MVI; VM-HCC+ (VETC+/MVI+, VETC-/MVI+, VETC+/MVI-); VM-HCC- (VETC-/MVI-); BCLC, Barcelona Clinic Liver Cancer; ALT, alanine aminotransferase; AST, aspartate aminotransferase; GGT, gamma-glutamyl transferase; ALB, albumin; PT, prothrombin time; PLT, platelet; AFP, alpha-fetoprotein; Tbil, total bilirubin.

https://doi.org/10.2147/JHC.S578689

selected feature in the optimal radiomics model (AP-IntraPeri5mm model) is illustrated in Supplemental Figure 2C. The features included in each of the nine radiomics models are summarized in Supplemental Table 2.

Model Construction and Comparison

The overall workflow for model development is illustrated in Figure 3. Based on the intratumoral, peritumoral, and intraperitumoral fusion features derived from the AP, PVP, and DP, nine radiomics models were constructed. The predictive performance of each model in the internal validation cohort is summarized in Table 3. Among the single-sequence models, the AP-IntraPeri model achieved the best predictive performance in the internal validation cohort, with an AUC of 0.756 (95% CI, 0.632–0.879). This finding suggests that integrating both intratumoral and peritumoral radiomics features enhanced the model's discriminative ability. The AP-IntraPeri model also demonstrated higher specificity and accuracy compared with the other radiomics models. Therefore, this model was combined with the clinical model to construct a clinical–radiomics combined model, which was subsequently evaluated in the external validation cohort.

The performance of the combined model in the external validation cohort is presented in Table 4, and the corresponding ROC curves for all datasets are shown in Figure 4. Compared with the single clinical model and the AP-IntraPeri model, the combined model exhibited superior predictive performance, achieving an AUC of 0.723 (95% CI, 0.625–0.821) in the external validation cohort. Calibration analysis and DCA demonstrated good agreement between predicted and observed probabilities (Supplemental Figure 3), as well as higher net clinical benefit for the combined model, supporting its potential clinical utility. According to the DeLong test (Supplemental Figure 4), the difference in AUCs between the combined model and the clinical model was statistically significant in the internal validation cohort ($P < 0.05$), whereas no significant differences were found among the other model pairs ($P > 0.05$). The variables included in the combined model were visualized using a nomogram (Supplemental Figure 5), which allows clinicians to estimate the probability of VM-HCC in individual patients based on serum AFP, ALB, and the tumor Rad-score.

Survival Prediction

All patients had complete follow-up. The median follow-up for the entire cohort was 30 months (range, 1–109 months), and disease progression was observed in 37.9% of patients (116/306). In the external validation cohort (n = 102), the median follow-up was 30 months (range, 1–96 months), and disease progression occurred in 48.0% of patients (49/102). Patients pathologically diagnosed with VM-HCC+ had significantly higher rates of ER than those with VM-HCC- (Log

Table 3 Predictive Performance of Different Models in the Internal Validation Cohort

Framework	AUC (95% CI)	Sensitivity (95% CI)	Specificity (95% CI)	Accuracy (95% CI)
AP-Intra model	0.712(0.582–0.842)	0.667(0478–0.814)	0.743(0.579–0.858)	0.710(0.587–0.808)
AP-Peri model	0.693(0.554–0.832)	0.667(0478–0.814)	0.743(0.579–0.858)	0.710(0.587–0.808)
AP-IntraPeri model	0.756(0.632–0.879)	0.667(0478–0.814)	0.800(0.641–0.900)	0.742(0.621–0.834)
PVP-Intra model	0.732(0.602–0.862)	0.741(0.553–0.868)	0.657(0.492–0.792)	0.694(0.570–0.794)
PVP-Peri model	0.653(0.513–0.793)	0.815 (0.633–0.918)	0.514(0.356–0.670)	0.645(0.521–0.753)
PVP-IntraPeri model	0.692(0.558–0.826)	0.889(0.719–0.961)	0.486(0.330–0.644)	0.661(0.537–0.767)
DP-Intra model	0.708(0.575–0.841)	0.778(0.592–0.894)	0.714(0.549–0.837)	0.742(0.621–0.834)
DP-Peri model	0.739(0.615–0.862)	0.519(0.340–0.693)	0.857(0.706–0.937)	0.710(0.587–0.808)
DP-IntraPeri model	0.708(0.579–0.837)	0.889(0.719–0.961)	0.543(0.382–0.695)	0.694(0.570–0.794)

Notes: Intra model, a model that combines features from single-sequence images within the tumor. Peri model, a model that combines features from single-sequence images surrounding the tumor. IntraPeri model, a model that integrates features from both the tumor and its surrounding microenvironment, incorporating characteristics from intra-tumoral and peri-tumoral single-sequence images.
Abbreviations: AUC, area under the receiver operating characteristic curve; AP, arterial phase; PP, portal-venous phase; DP, delayed phase. CI, confidence interval.

Table 4 Diagnostic Performance of Clinic Model, AP-IntraPeri Model and Combined Model in the Training Cohort, Internal Validation Cohort and External Validation Cohort

Framework	AUC (95% CI)	Sensitivity(95% CI)	Specificity (95% CI)	Accuracy (95% CI)
Training				
Clinical model	0.680(0.594–0.765)	0.696(0.567–0.801)	0.605(0.499–0.701)	0.641(0.559–0.715)
AP-IntraPeri model	0.839(0.772–0.906)	0.696(0.567–0.801)	0.895(0.813–0.944)	0.817(0.745–0.872)
Combined model	0.857(0.795–0.919)	0.857(0.747–0.927)	0.744(0.639–0.822)	0.789(0.714–0.848)
Internal validation				
Clinical model	0.593(0.456–0.730)	0.333(0.186–0.522)	0.857(0.706–0.937)	0.629(0.505–0.738)
AP-IntraPeri model	0.756(0.632–0.879)	0.667(0.478–0.814)	0.800(0.641–0.900)	0.742(0.621–0.834)
Combined model	0.761(0.642–0.880)	0.778(0.592–0.894)	0.657(0.492–0.792)	0.710(0.587–0.808)
External validation				
Clinical model	0.617(0.518–0.716)	0.574(0.442–0.697)	0.646(0.504–0.766)	0.608(0.511–0.697)
AP-IntraPeri model	0.700(0.599–0.801)	0.537(0.406–0.663)	0.812(0.681–0.898)	0.667(0.571–0.751)
Combined model	0.723(0.625–0.821)	0.500(0.371–0.629)	0.917(0.804–0.967)	0.696(0.601–0.777)

Notes: IntraPeri model, a model that integrates features from both the tumor and its surrounding microenvironment, incorporating characteristics from intra-tumoral and peri-tumoral single-sequence images. Combined model, which combined the features of AP-IntraPeri model and clinical model.
Abbreviations: AUC, area under the receiver operating characteristic curve; AP, arterial phase. CI, confidence interval.

rank test, P = 0.00037) and exhibited markedly shorter DFS (Log rank test, P = 0.00015) (Figure 5A and C). A similar prognostic trend was observed when patients were stratified according to the combined model's predicted results (Figure 5B and D). Prognostic associations were primarily evaluated in the external validation cohort as an independent test set to minimize optimism bias, with supportive analyses in the overall cohort (Supplemental Figure 6). When patients were stratified into four vascular-pattern subgroups (VETC−/MVI−, n=169; VETC−/MVI+, n=97; VETC+/MVI−, n=18; VETC+/MVI+, n=22), Kaplan–Meier analyses showed significant differences across groups for ER (overall Log rank test P=0.000151) and DFS (overall Log rank test P=0.000242) (Supplemental Figure 7). Pairwise comparisons indicated that MVI-positive subgroups (VETC−/MVI+ and VETC+/MVI+) had worse outcomes than the double-negative subgroup, whereas VETC+/MVI− did not significantly differ from VETC−/MVI− for either endpoint (ER P=0.464; DFS P=0.511).

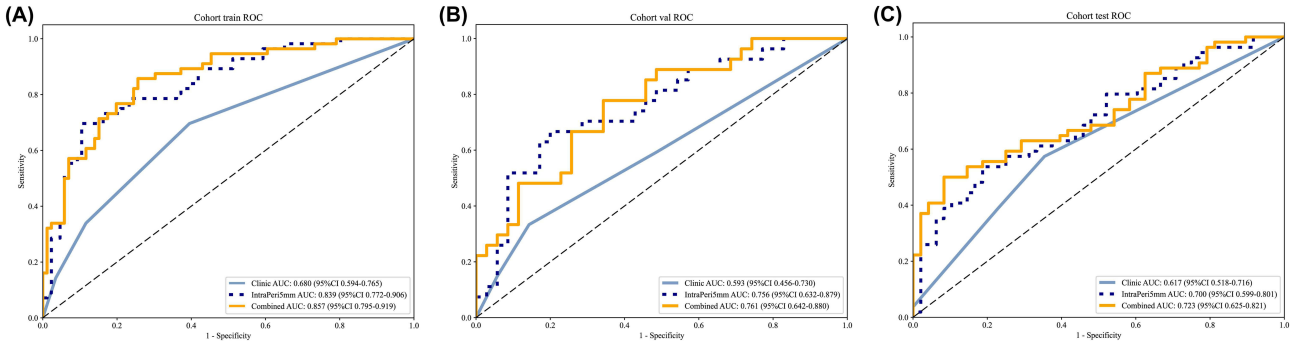

Figure 4 Assessment of models for the ability to predict VM-HCC.
Notes: ROCs of models in training cohort (**A**) internal validation cohort (**B**) and external validation cohort (**C**). IntraPeri model, a model that integrates features from both the tumor and its surrounding microenvironment, incorporating characteristics from intra-tumoral and peri-tumoral single-sequence images. Combined model, which combined the features of AP-IntraPeri model and clinical model.
Abbreviations: HCC, hepatocellular carcinoma; VETC, vessels encapsulating tumor clusters; MVI, microvascular invasion; VM, VETC-MVI; ROC, receiver operating characteristic.

https://doi.org/10.2147/JHC.S578689

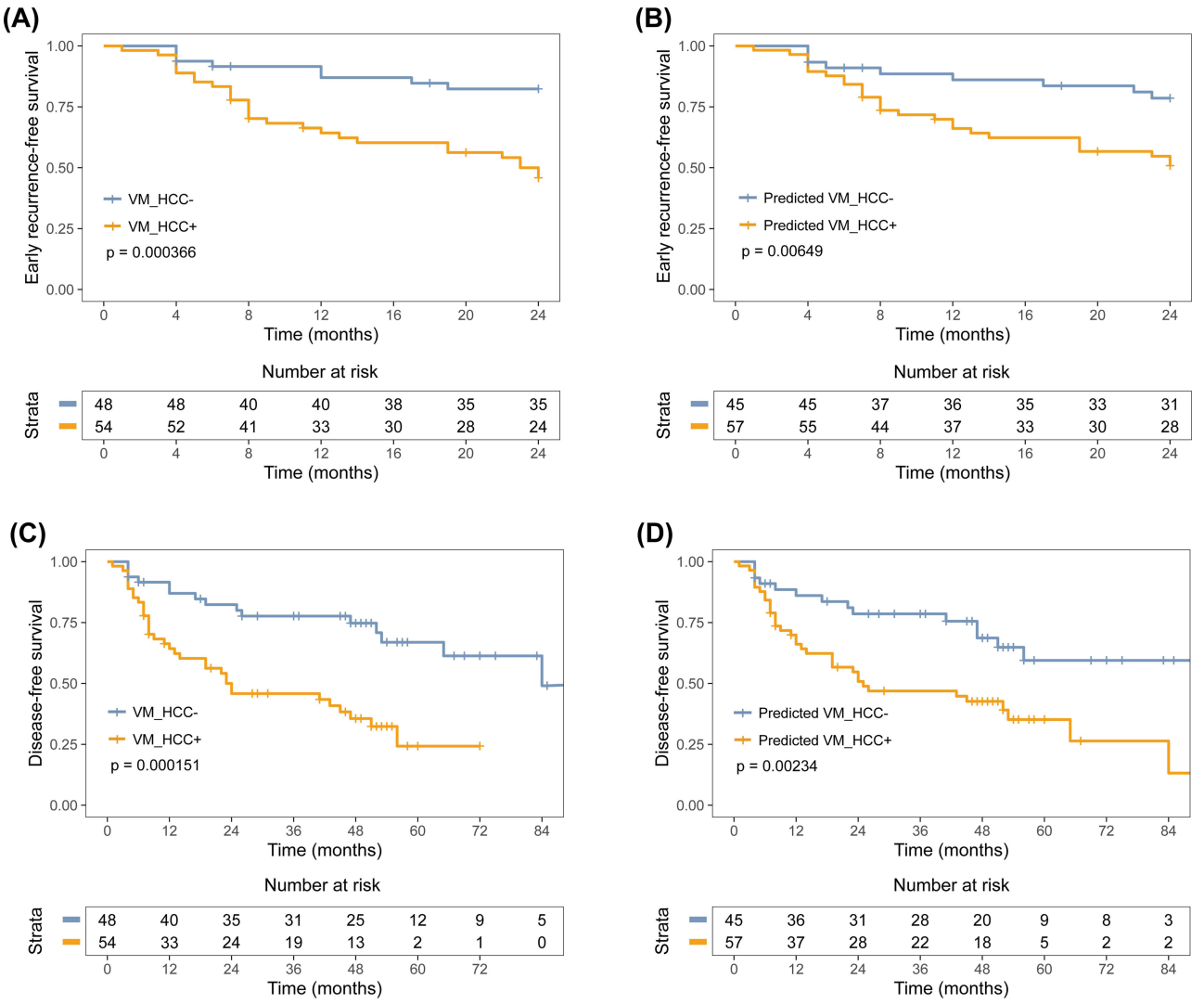

Figure 5 Kaplan–Meier curves of early recurrence-free survival and disease-free survival in the outcome cohort.
Notes: ER curves and DFS curves stratified by histologic VM-HCC pattern (**A** and **C**) and combined model-predicted VM-HCC pattern (**B** and **D**), presented through Kaplan–Meier analysis. Statistical comparisons between different models were performed by using the Log rank test.
Abbreviations: HCC, hepatocellular carcinoma; VETC, vessels encapsulating tumor clusters; MVI, microvascular invasion; VM, VETC-MVI; VM-HCC+ (VETC+/MVI+, VETC-/MVI+, VETC+/MVI-) and VM-HCC- (VETC-/MVI-). ER, early recurrence; DFS, disease-free survival.

The double-positive subgroup exhibited the poorest prognosis and differed significantly from the VETC+/MVI− subgroup (ER p=0.00307; DFS p=0.00451). In multivariable Cox regression, VM-HCC remained independently associated with DFS (HR 1.42, 95% CI 1.03–1.95; P=0.032). However, the association between VM-HCC and ER did not reach statistical significance after adjustment (HR 1.40, 95% CI 0.94–2.09; P=0.093). Tumor size and albumin status were independent predictors for both ER and DFS (Supplemental Table 3).

Discussion

This study developed and externally validated a DCE-MRI–based clinical–radiomics model for preoperative prediction of VM-HCC. In the internal validation cohort, the combined model formed by the AP-IntraPeri model and clinical model achieved an AUC of 0.761 (95% CI: 0.642–0.880), outperforming other models. In the external validation cohort, the combined model achieved an AUC of 0.723 (95% CI: 0.625–0.821), demonstrating good cross-center generalizability. Moreover, model-predicted VM positivity was significantly associated with early recurrence and shorter disease-free survival, underscoring its potential value for preoperative risk stratification.

EMT is a recognized mechanism underlying HCC invasion and metastasis.[20] In clinical practice, MVI is closely associated with EMT and has been confirmed as an important predictor of poor prognosis, including tumor recurrence and overall survival (OS) in HCC patients.[11] However, a significant proportion of patients with negative MVI still experience recurrence, suggesting that relying solely on MVI is insufficient to fully reflect the tumor's invasive potential.[21] Fang et al identified a unique angiogenic pattern, independent of EMT, termed "vessels encapsulating tumor clusters", which may represent a new therapeutic target for HCC.[10,22] Subsequent studies have shown that VETC is closely related to MVI and serves as an important predictor of rapid tumor progression in HCC.[9] A large multicenter study[6] also demonstrated the complementary value of VETC in predicting recurrence, highlighting that the combined analysis of both vascular patterns can offer a more comprehensive representation of tumor heterogeneity and improve the accuracy of recurrence risk assessment. While previous imaging studies primarily focused on MVI,[23,24] recent studies have attempted to evaluate MVI and VETC jointly.[16,17,25,26] Zhu et al identified an AFP level higher than 400 ng/mL, a nonsmooth tumor margin, and peritumoral arterial enhancement as independent predictors of VM-HCC, with VM pattern being closely associated with early recurrence of HCC.[25] Yang et al[16] constructed a combined model by integrating radiomics features from three DCE-MRI phases, including AP, PVP and DP, with clinical variables to effectively assess VM-HCC patterns, with the results correlated with ER and progression-free survival (PFS). Another study[17] combined the VM pattern of HCC, MR radiomics, and deep learning methods to construct a DeepSurv model for evaluating recurrence-free survival (RFS) after curative hepatectomy. This model was compared with other clinical and radiomics models, demonstrating promising performance and good feasibility.

Compared with previous studies, our research further integrated intratumoral and peritumoral radiomics features derived from the arterial phase to construct a comprehensive model aimed at characterizing VM patterns in HCC. Given that most MVI occurs in the peritumoral region,[18] and that VETC is biologically related to vascular remodeling, the inclusion of peritumoral information is biologically plausible. Previous studies have also demonstrated that the combined analysis of intra- and peritumoral radiomics features improves prediction accuracy for pathological differentiation,[27] microvascular invasion,[28] and prognosis[29] in HCC. In our study, our fusion model based on DCE-MRI arterial-phase intratumoral and peritumoral features may provide a more comprehensive imaging representation of tumor heterogeneity and vascular-related characteristics. Additionally, our results demonstrate that inclusion of 5-mm peritumoral features improves model performance, consistent with previous findings.[23,30,31] This peritumoral range may be particularly sensitive to microenvironmental alterations while reducing interference from adjacent normal liver tissue, although this interpretation remains inferential. Nevertheless, associations between specific radiomic signatures and VM biology remain inferential rather than mechanistic.

In our study, we also identified key clinical and radiomics predictors of VM-HCC and compared the performance of phase-specific DCE-MRI radiomics models. Clinical factor analysis identified AFP > 200 ng/mL and ALB > 40 g/L as independent predictors of VM-HCC+, supporting their role in reflecting tumor invasiveness and recurrence risk. Consistent with the findings of previous studies,[31–34] this further validates the clinical significance of these indicators in reflecting tumor invasiveness and recurrence risk. Furthermore, we found that the radiomics model constructed from AP DCE-MRI data outperformed models based on PVP and DP data in predicting VM-HCC. This result also aligns with a previous study.[35] Another radiomics study based on multiphase DCE-MRI used features from T1WI, AP, PVP and DP, and compared single-phase and all-phase models. The all-phase model outperformed the single-phase model, with the arterial phase contributing significantly to the model.[36] Collectively, these findings may suggest that the arterial phase can more directly reflect the tumor vascularity and neovascularization of HCC, thereby providing imaging features that are particularly sensitive to perfusion dynamics and intratumoral heterogeneity. Nevertheless, several studies[16,37] have reported that models derived from the portal venous phase or multiphase fused datasets may achieve comparable or even superior performance. Meanwhile, we found that combined models integrating radiomic features with clinical parameters generally demonstrate higher discriminative ability and greater clinical net benefit in prognostic evaluation and risk stratification than models based solely on imaging or clinical data. These results highlight that the incorporation of clinical information is a key approach to enhancing the clinical applicability of radiomics-based models for HCC.

In summary, the key incremental value of our study lies in the explicit integration of intra- and peritumoral arterial-phase DCE-MRI features, the construction of a combined nomogram incorporating basic clinical predictors (AFP, ALB), and rigorous validation in an independent external cohort.

ER after surgical resection remains a major challenge affecting long-term survival in patients with HCC. In this study, patients with VM-HCC+ demonstrated a significantly higher risk of ER and shorter DFS, suggesting that the preoperatively predicted VM pattern may have potential value in recurrence risk stratification. To address potential heterogeneity within the composite VM definition, we further examined prognostic differences across the four VETC/MVI histologic patterns. In our cohorts, patients with concurrent VETC and MVI had the worst outcomes, whereas the VETC+/MVI− subgroup did not differ significantly from the VETC−/MVI− subgroup. Given the small sample size of the VETC+/MVI− group, these subgroup results should be interpreted as exploratory and supportive. After multivariable adjustment, VM-HCC remained independently associated with shorter DFS, supporting the complementary prognostic value of combined vascular-pattern assessment. This aligns with prior studies integrating VETC and MVI for recurrence-risk modeling, where combined vascular-pattern assessment improves prognostic stratification.[6] Tumor size and albumin level were also independently associated with outcomes, reflecting the combined influence of tumor burden and host condition.[38]

For patients predicted to have VM-HCC+, early postoperative adjuvant therapies—such as TACE or antiangiogenic targeted treatment—could be hypothesized as potential strategies to mitigate recurrence risk.[22,39,40] However, these implications remain speculative and require prospective validation.

This study has several limitations. First, it was designed as a retrospective study, which may have introduced selection bias. Second, all enrolled patients had resectable HCC; therefore, our findings primarily reflect the biological characteristics of surgical cases and may not be generalizable to patients with unresectable or advanced HCC. Third, as our cohorts mainly included Asian patients with HBV-related HCC, external validation in ethnically and etiologically diverse populations is required to further establish the model's generalizability. Fourth, radiomics features were extracted solely from arterial phase DCE-MRI images without integrating multiphase dynamic contrast-enhanced data, which may limit the comprehensive characterization of hemodynamic heterogeneity across different enhancement phases. Future studies should involve larger, multicenter, and prospective cohorts with diverse etiological backgrounds, and integrate multimodal radiomics with genomic or next-generation sequencing data to further improve the biological interpretability and predictive performance of the model, thereby providing a more robust foundation for precision treatment of HCC.

Conclusion

The clinical–radiomics model based on the fusion of intra- and peritumoral arterial phase features demonstrated good robustness and external validity for predicting the VM pattern in HCC. Our study provides a useful noninvasive tool for risk stratification and individualized management of HCC patients.

Abbreviations

AFP, alpha-fetoprotein; ALB, albumin; ALT, alanine aminotransferase; AP, arterial phase; AST, aspartate aminotransferase; AUC, area under the receiver operating characteristic curve; BCLC, Barcelona Clinic Liver Cancer; CI, confidence interval; CT, computed tomography; DCA, decision curve analysis; DCE-MRI, dynamic contrast-enhanced magnetic resonance imaging; DFS, disease-free survival; DP, delayed phase; EMT, epithelial-mesenchymal transition; ER early recurrence; Gd-BOPTA, gadobenate dimeglumine; GGT, gamma-glutamyl transferase; HBV, hepatitis B virus; HCC, hepatocellular carcinoma; ICC, intraclass correlation coefficient; LASSO, least absolute shrinkage and selection operator; MVI, microvascular invasion; OR, odds ratio; PFS, progression-free survival; PP, portal-venous phase; PT, prothrombin time; RAD, score radiomics score; RFS, recurrence-free survival; ROC, receiver operating characteristic; ROI, region of interest; SD, standard deviation; TACE, transarterial chemoembolization; VETC, vessels encapsulating tumor cluster; VIF, variance inflation factor; VM, VETC and MVI.

Data Sharing Statement

The datasets used and analyzed during the current study are available from the corresponding author upon reasonable request.

Ethics Approval and Informed Consent

The study was conducted in accordance with the Declaration of Helsinki. The study was endorsed by the ethical review committee of Beijing YouAn Hospital, Capital Medical University (LL-2019-139-K). Since this was a retrospective study, the requirement for obtaining informed consent from patients was waived upon approval by the ethics committee. Data collection and processing were conducted in strict compliance with patient privacy protection principles. All personally identifiable information was fully anonymized, with direct identifiers (including name, ID number, contact information, etc.) removed to ensure that no individual patient could be identified by readers.

Consent for Publication

All the authors agreed to publish the article.

Acknowledgment

We sincerely thank Platform Onekey AI for Code consultation of the study.

Author Contributions

All authors made a significant contribution to the work reported, whether that is in the conception, study design, execution, acquisition of data, analysis and interpretation, or in all these areas; took part in drafting, revising or critically reviewing the article; gave final approval of the version to be published; have agreed on the journal to which the article has been submitted; and agree to be accountable for all aspects of the work.

Funding

This work was supported by Beijing Hospital Authority Clinical Medicine Development special funding support (No. ZLRK202333); the National Natural Science Foundation of China (No. 61936013, No. 82271963);the Beijing Municipal Natural Science Foundation (No. 7212051, No. L222097); Scientific Research Project of Beijing Youan Hospital, CCMU, 2024.

Disclosure

The authors report no conflicts of interest in this work.

References

1. Sung H, Ferlay J, Siegel RL, et al. Global cancer statistics 2020: GLOBOCAN estimates of incidence and mortality worldwide for 36 cancers in 185 countries. *CA Cancer J Clin*. 2021;71(3):209–249. doi:10.3322/caac.21660
2. Brown ZJ, Tsilimigras DI, Ruff SM, et al. Management of hepatocellular carcinoma: a review. *JAMA Surg*. 2023;158(4):410–420. doi:10.1001/jamasurg.2022.7989
3. Vogel A, Meyer T, Sapisochin G, Salem R, Saborowski A. Hepatocellular carcinoma. *Lancet*. 2022;400(10360):1345–1362. doi:10.1016/S0140-6736(22)01200-4
4. Morse MA, Sun W, Kim R, et al. The role of angiogenesis in hepatocellular carcinoma. *Clin Cancer Res*. 2018;25(3):912–920. doi:10.1158/1078-0432.CCR-18-1254
5. Lu L, Wei W, Huang C, et al. A new horizon in risk stratification of hepatocellular carcinoma by integrating vessels that encapsulate tumor clusters and microvascular invasion. *Hepatol Int*. 2021;15(3):651–662. doi:10.1007/s12072-021-10183-w
6. Lin W-P, Xing K-L, Fu J-C, et al. Development and validation of a model including distinct vascular patterns to estimate survival in hepatocellular carcinoma. *JAMA Network Open*. 2021;4(9):e2125055. doi:10.1001/jamanetworkopen.2021.25055
7. Wan L, Pantel K, Kang Y. Tumor metastasis: moving new biological insights into the clinic. *Nat Med*. 2013;19(11):1450–1464. doi:10.1038/nm.3391
8. Liu K, Dennis C, Prince DS, et al. Vessels that encapsulate tumour clusters vascular pattern in hepatocellular carcinoma. *JHEP Rep*. 2023;5(8):100792. doi:10.1016/j.jhepr.2023.100792
9. Renne SL, Woo HY, Allegra S, et al. Vessels Encapsulating Tumor Clusters (VETC) Is a powerful predictor of aggressive hepatocellular carcinoma. *Hepatology*. 2019;71(1):183–195. doi:10.1002/hep.30814
10. Fang J-H, Zhou H-C, Zhang C, et al. A novel vascular pattern promotes metastasis of hepatocellular carcinoma in an epithelial-mesenchymal transition-independent manner. *Hepatology*. 2015;62(2):452–465. doi:10.1002/hep.27760
11. Lee S, Kang TW, Song KD, et al. Effect of microvascular invasion risk on early recurrence of hepatocellular carcinoma after surgery and radiofrequency ablation. *Ann Surg*. 2021;273(3):564–571. doi:10.1097/SLA.0000000000003268
12. Xu X-F, Diao Y-K, Zeng -Y-Y, et al. Association of severity in the grading of microvascular invasion with long-term oncological prognosis after liver resection for early-stage hepatocellular carcinoma: a multicenter retrospective cohort study from a hepatitis B virus-endemic area. *Int J Surg*. 2023;109(4):841–849. doi:10.1097/JS9.0000000000000325

13. Xia T, Zhao B, Li B, et al. MRI-Based radiomics and deep learning in biological characteristics and prognosis of hepatocellular carcinoma: opportunities and challenges. *J Magn Reson Imaging*. 2023;59(3):767–783. doi:10.1002/jmri.28982
14. Tomaszewski MR, Gillies RJ. The biological meaning of radiomic features. *Radiology*. 2021;298(3):505–516. doi:10.1148/radiol.2021202553
15. Bera K, Braman N, Gupta A, Velcheti V, Madabhushi A. Predicting cancer outcomes with radiomics and artificial intelligence in radiology. *Nat Rev Clin Oncol*. 2021;19(2):132–146. doi:10.1038/s41571-021-00560-7
16. Yang J, Dong X, Jin S, et al. Radiomics model of dynamic contrast-enhanced MRI for evaluating vessels encapsulating tumor clusters and microvascular invasion in hepatocellular carcinoma. *Acad Radiol*. 2024;32(1):146–156. doi:10.1016/j.acra.2024.07.007
17. Zhang C, L-d M, Zhang X-L, et al. Magnetic resonance deep learning radiomic model based on distinct metastatic vascular patterns for evaluating recurrence-free survival in hepatocellular carcinoma. *J Magn Reson Imaging*. 2023;60(1):231–242. doi:10.1002/jmri.29064
18. Roayaie S, Blume IN, Thung SN, et al. A system of classifying microvascular invasion to predict outcome after resection in patients with hepatocellular carcinoma. *Gastroenterology*. 2009;137(3):850–855. doi:10.1053/j.gastro.2009.06.003
19. Marrero JA, Kulik LM, Sirlin CB, et al. Diagnosis, staging, and management of hepatocellular carcinoma: 2018 practice guidance by the American Association for the Study of Liver Diseases. *Hepatology*. 2018;68(2):723–750. doi:10.1002/hep.29913
20. Giannelli G, Koudelkova P, Dituri F, Mikulits W. Role of epithelial to mesenchymal transition in hepatocellular carcinoma. *J Hepatol*. 2016;65(4):798–808. doi:10.1016/j.jhep.2016.05.007
21. Portolani N, Baiocchi GL, Molfino S, Benetti A, Gheza F, Giulini SM. Microvascular infiltration has limited clinical value for treatment and prognosis in hepatocellular carcinoma. *World J Surg*. 2014;38(7):1769–1776. doi:10.1007/s00268-013-2426-6
22. Fang J-H, Xu L, Shang L-R, et al. Vessels That Encapsulate Tumor Clusters (VETC) pattern is a predictor of sorafenib benefit in patients with hepatocellular carcinoma. *Hepatology*. 2019;70(3):824–839. doi:10.1002/hep.30366
23. Xia T-Y, Zhou Z-H, Meng X-P, et al. Predicting microvascular invasion in hepatocellular carcinoma using CT-based radiomics model. *Radiology*. 2023;307(4):e222729. doi:10.1148/radiol.222729
24. Xu X, Zhang H-L, Liu Q-P, et al. Radiomic analysis of contrast-enhanced CT predicts microvascular invasion and outcome in hepatocellular carcinoma. *J Hepatol*. 2019;70(6):1133–1144. doi:10.1016/j.jhep.2019.02.023
25. Zhu Y, Yang L, Wang M, et al. Preoperative MRI features to predict vessels that encapsulate tumor clusters and microvascular invasion in hepatocellular carcinoma. *Eur J Radiol*. 2023;167:111089. doi:10.1016/j.ejrad.2023.111089
26. Yang J, Dong X, Wang G, et al. Preoperative MRI features for characterization of vessels encapsulating tumor clusters and microvascular invasion in hepatocellular carcinoma. *Abdom Radiol*. 2022;48(2):554–566. doi:10.1007/s00261-022-03740-w
27. Liu H-F, Wang M, Wang Q, et al. Multiparametric MRI-based intratumoral and peritumoral radiomics for predicting the pathological differentiation of hepatocellular carcinoma. *Insights Imaging*. 2024;15(1):97. doi:10.1186/s13244-024-01623-w
28. Li Y, Li H, Feng Y, Lu L, Zhang J, Jia N. Intratumoral and peritumoral radiomics based on DCE-MRI for prediction of microvascular invasion grading in solitary hepatocellular carcinoma (≤3 cm). *J Hepatocell Carcinoma*. 2025;12:1083–1095. doi:10.2147/JHC.S519578
29. Li J, Zhou M, Tong Y, et al. Tumor growth pattern and intra- and peritumoral radiomics combined for prediction of initial TACE outcome in patients with primary hepatocellular carcinoma. *J Hepatocell Carcinoma*. 2024;11:1927–1944. doi:10.2147/JHC.S480554
30. Wang F, Cheng M, Du B, et al. Predicting microvascular invasion in small (≤ 5 cm) hepatocellular carcinomas using radiomics-based peritumoral analysis. *Insights Imaging*. 2024;15(1):90. doi:10.1186/s13244-024-01649-0
31. Wang K-D, Guan M-J, Bao Z-Y, et al. Radiomics analysis based on dynamic contrast-enhanced MRI for predicting early recurrence after hepatectomy in hepatocellular carcinoma patients. *Sci Rep*. 2025;15(1):22240. doi:10.1038/s41598-025-02291-6
32. Li W-F, Yen Y-H, Liu Y-W, et al. Preoperative predictors of early recurrence after resection for hepatocellular carcinoma. *Am J Surg*. 2021;223(5):945–950. doi:10.1016/j.amjsurg.2021.08.012
33. Zhang K, Tao C, Siqin T, Wu J, Rong W. Establishment, validation and evaluation of predictive model for early relapse after R0 resection in hepatocellular carcinoma patients with microvascular invasion. *J Transl Med*. 2021;19(1):293. doi:10.1186/s12967-021-02940-0
34. Chang Y-S, Tsai M-J, Tsai C-J, et al. A new model based on preoperative AFP, albumin, and tumor burden score for predicting microvascular invasion in early-stage HCC. *Am J Cancer Res*. 2024;14(10):4979–4988. doi:10.62347/ZGRJ7827
35. Zhang J, Liu M, Qu Q, et al. Radiomics analysis of gadoxetic acid-enhanced MRI for evaluating vessels encapsulating tumour clusters in hepatocellular carcinoma. *Front Oncol*. 2024;14:1422119. doi:10.3389/fonc.2024.1422119
36. Sun K, Shi L, Qiu J, Pan Y, Wang X, Wang H. Multi-phase contrast-enhanced magnetic resonance image-based radiomics-combined machine learning reveals microscopic ultra-early hepatocellular carcinoma lesions. *Eur J Nucl Med Mol Imaging*. 2022;49(8):2917–2928. doi:10.1007/s00259-022-05742-8
37. Dong X, Yang J, Zhang B, et al. Deep learning radiomics model of dynamic contrast-enhanced mri for evaluating vessels encapsulating tumor clusters and prognosis in hepatocellular carcinoma. *J Magn Reson Imaging*. 2023;59(1):108–119. doi:10.1002/jmri.28745
38. Nevola R, Ruocco R, Criscuolo L, et al. Predictors of early and late hepatocellular carcinoma recurrence. *World J Gastroenterol*. 2023;29(8):1243–1260. doi:10.3748/wjg.v29.i8.1243
39. Peng Z, Chen S, Xiao H, et al. Microvascular invasion as a predictor of response to treatment with sorafenib and transarterial chemoembolization for recurrent intermediate-stage hepatocellular carcinoma. *Radiology*. 2019;292(1):237–247. doi:10.1148/radiol.2019181818
40. Wang J-H, Li X-S, Tang H-S, et al. Vessels that encapsulate tumor clusters (VETC) pattern predicts the efficacy of adjuvant TACE in hepatocellular carcinoma. *J Cancer Res Clin Oncol*. 2022;149(8):4163–4172. doi:10.1007/s00432-022-04323-4